Q. J. R. Meteorol. Soc. (2002), **128**, pp. 2059–2072

Comparison of probability density functions for total specific humidity and saturation deficit humidity, and consequences for cloud parametrization

By JEREMY D. PRICE[1]* and ROBERT WOOD[2]
[1]*Met Office, UK*
[2]*University of Washington, USA*

(Received 24 May 2001; revised 5 April 2002)

SUMMARY

Various models which predict cloud variables use probability density functions of either specific humidity or saturation deficit humidity to represent subgrid-scale variations. Using the former is considered to be an approximation since it does not allow variation of dew-point across the grid. In this paper the validity of that approximation is investigated and typical errors incurred are stated. Aircraft data from subtropical regions and tethered-balloon data from midlatitudes are examined to compare differences between the two types of distribution. The average relative error in cloud fraction introduced by assuming a constant value of saturation across a grid is found to be approximately half an okta. However, results suggest that there is a fixed relation between the widths of both distributions allowing easy conversion between the two.

KEYWORDS: Cloud modelling Humidity observations

1. INTRODUCTION

The origins of statistical cloud schemes which use a probability density function (PDF) to represent the subgrid-scale humidity variation date back to Sommeria and Deardorff (1977) and Mellor (1977). Later work introduced a variety of relations to define the PDF, including rectangular, triangular, Gaussian and skewed forms (Smith 1990; Le-Treut and Li 1991; Ek and Mahrt 1991; Ricard and Royer 1993; Cuijpers and Bechtold 1995; Cusack *et al.* 1999; Lohmann *et al.* 1999; Tompkins 2002). Currently there appear to be few detailed observational studies describing humidity PDFs which can be used to validate assumptions made in atmospheric models. Price (2001) and Larson *et al.* (2001) have examined tethered-balloon and aircraft data, respectively, to characterize typical humidity distributions. Their work considered the importance of humidity distributions when estimating cloud parameters from parametrizations, and concluded that incomplete modelling of humidity PDFs significantly increases errors in predicted variables. Pincus and Klein (2000) reached a similar conclusion argued on theoretical grounds.

Currently most statistical schemes use distributions in either total specific humidity, q_t, or saturation deficit, $q_t - q_{sat}$, where q_{sat} is the saturated specific humidity. The saturation deficit is a measure of the thermodynamic distance of an air parcel from saturation, which may be expected to provide the most accurate predictions since it also allows subgrid-scale variation in q_{sat} and, crucially, includes its spatial correlation with q_t. However, this spatial correlation does not appear to have been verified experimentally, so that it is presently unclear whether models using distributions in $q_t - q_{sat}$ have any real advantage over those using q_t.

Previous work, therefore, has not conducted any systematic comparison of observed q_t and $q_t - q_{sat}$ distributions to assess which may be more suitable for predicting cloud parameters. The present paper examines observational data (collected from aircraft and tethered-balloon platforms) to perform a comparison of PDFs for total specific humidity and saturation deficit humidity. This includes a calculation for the relative errors in cloud

* Corresponding author: Met. Research Unit, Cardington Airfield, Shortstown, Bedforshire MK42 0SY, UK.
e-mail: jeremy.price@metoffice.com

fraction incurred when using PDFs of either q_t or $q_t - q_{sat}$. The results are used to discuss the suitability of each variable for cloud parametrization schemes. Section 2 describes the data and analysis used, section 3 presents the results, and section 4 is a summary.

2. Data

The study uses data from two facilities operated by the UK Met Office: the C130 research aircraft, and the large-tethered-balloon facility. C130 data are from the First International Satellite Cloud Climatology Project Regional Experiment (FIRE, Randall *et al.* 1984), the Atlantic Stratocumulus Transition Experiment (ASTEX, Bretherton and Pincus 1995) and the Journal of Atmospheric Sciences special ASTEX issue (1995, volume 52 No. 16); and the South Atlantic Tropospheric Experiment (SATE-2, Francis and Taylor 1995). All of these campaigns were based in subtropical regions over the ocean, and data represent cloudy marine boundary layers containing stratocumulus (Sc), cumulus (Cu) and Cu rising into Sc (CuSc). Data from 30 flights were used constituting a total of 319 aircraft runs which were typically 50–100 km long. Runs were performed in both clear air and cloud, and are described in more detail in Wood and Field (2000). Details of the sensors used (a total water detector and a Rosemount platinum resistance thermometer) are given in Rogers *et al.* (1995). Data used from the tethered-balloon facility were collected at three locations in the UK: Cardington in Bedfordshire, South-East England (51°40′N, 1°20′W); Andover in Hampshire, southern England (51°36′N, 1°18′W); and Sennybridge in Powys, Wales (52°01′N, 3°34′W). Data were collected at various heights up to the maximum ceiling of 1.8 km. The majority were in the boundary layer, but a significant number of time series were collected above this. Data were mostly collected in clear air, either in clear conditions or above or below cloud. However, a significant proportion of the data were collected from inside cloud using the total water probe. Time series of humidity and temperature were divided into sectors which represented an advective length-scale ranging from 2 to 20 km. Data were used from 12 days at typically two or three different heights. In total 61 data sectors were used, representing a reasonably wide range of conditions and seasons over land at midlatitudes (strong cyclonic conditions were not sampled). Details of the tethered-balloon sensors (also a total water detector and platinum resistance thermometer) can be found in Lapworth and Mason (1988) and Price *et al.* (1998).

All the data were, therefore, collected in or near the boundary layer and are thus relevant to the forecasting of low cloud and fog.

3. Results

(*a*) *Comparison of moments*

In this section a comparison of the second (standard deviation, σ), third (skewness, S) and fourth (kurtosis, K) moments between distributions of q_t and $q_t - q_{sat}$ is performed. The results are summarized in Tables 1 to 3. Some aircraft data were discarded due to the presence of anomalous values; where this happened is indicated in the tables. Table 1 shows that respective values of standard deviation are quite similar for both aircraft and balloon data, despite almost an order of magnitude difference in the length-scale between the two. One would expect aircraft observations of greater length-scales to show a larger standard deviation due to the presence of mesoscale gradients. However, the tethered-balloon data include a significant number of more turbulent convectively unstable cases which also normally show a large standard deviation (Price 2001). The agreement may therefore be coincidental. The values for S and K in Table 1 show

TABLE 1. AVERAGE SECOND, THIRD AND FOURTH MOMENTS WITH STANDARD DEVIATIONS FOR ALL AIRCRAFT AND TETHERED-BALLOON DATA

	σ_{qt}	S_{qt}	K_{qt}	σ_{qsat}	S_{qsat}	K_{qsat}	$\sigma_{qt-qsat}$	$S_{qt-qsat}$	$K_{qt-qsat}$
Aircraft average	0.28	0.20	3.38*	0.14	-0.18^{+}	3.69^{+}	0.37	0.14^{+}	3.58^{+}
σ	0.19	2.09	1.56*	0.12	0.73^{+}	1.76^{+}	0.29	0.78^{+}	1.70^{+}
Tethered-balloon average	0.30	−0.05	3.19	0.19	0.08	3.02	0.38	−0.06	2.98
σ	0.32	0.83	1.38	0.16	0.64	1.35	0.41	0.72	1.23

S is skewness, K is kurtosis, q_t is the total specific humidity, and $q_t - q_{sat}$ is the saturation deficit.
* 6% bad data points removed;
$^{+}$ 13% bad data points removed.

TABLE 2. AVERAGE RATIO OF MOMENTS FOR ALL AIRCRAFT AND TETHERED-BALLOON DATA WITH STANDARD DEVIATION AND STANDARD ERROR

	$\sigma_{qt}/\sigma_{qt-qsat}$	$S_{qt}/S_{qt-qsat}$	$K_{qt}/K_{qt-qsat}$	Cloud error
Aircraft	0.80	0.61^{+}	0.99^{+}	–
σ	0.21	1.65	0.28	–
Standard Error	0.01	0.10	0.02	
Tethered balloon	0.81	1.44	1.12	0.057
σ	0.71	1.65	0.45	0.049
Standard Error	0.09	0.21	0.06	

The cloud error (discussed in section 3(c)) is the average of 61 mean values from the tethered-balloon data series. S is skewness, K is kurtosis, q_t is total specific humidity, and $q_t - q_{sat}$ the saturation deficit.
$^{+}$ 13% bad data points removed.

values of approximately 0 and 3 (the aircraft data showing slightly greater deviation from these values than the balloon). On average therefore, humidity distributions are close to Gaussian in nature. Note, however, that the standard deviations of the third and fourth moments in Table 1 are large, and in fact most individual observations are not Gaussian (Price 2001; Larson *et al.* 2001).

Table 2 shows the average ratios of the moments defined as:

$$\overline{\frac{x_{qt}}{x_{qt-qsat}}} = \frac{1}{n}\sum^{n}\frac{x_{qt}}{x_{qt-qsat}},$$

where x is the moment under investigation. The results show that $\sigma_{qt}/\sigma_{qt-qsat}$ is not significantly different for the two datasets, and that both show similar ratios for kurtosis of near unity, though that for the balloon data appears a little larger. However, skewness does show a significant difference, with the balloon data showing greater skewness in q_t than in $q_t - q_{sat}$, which is the opposite to the aircraft data. The reason for this is not clear, but there is no evidence to suggest the result is due to instrumental bias. Therefore it is possible the subtropical data may have a significantly different morphology to midlatitudes. Note that the standard deviations of the ratios, with the exception of skewness, are larger for tethered-balloon data, which most likely reflects the increased variety of conditions sampled. Also note that the fact that the ratio $\sigma_{qt}/\sigma_{qt-qsat}$ is consistent between datasets, which suggests that there may be a general proportionality between the two (see below). The results show that most of the variations in the moments of the $q_t - q_{sat}$ distribution (apart from skewness) are due to those in the distribution of q_t.

Figures 1–3 show scatter plots of σ, S and K for aircraft data. Panels (a) and (b) show the ratios of $q_{\rm sat}$ moments to $q_{\rm t}$ and $q_{\rm t} - q_{\rm sat}$ moments respectively. It is clear from these diagrams that moments of $q_{\rm sat}$ do not show a strong relation to either those of $q_{\rm t}$ or $q_{\rm t} - q_{\rm sat}$. The distribution of $q_{\rm sat}$, therefore, appears to be relatively independent. Panels (c) in the figures are consistent with the results in Table 2 and also illustrate that most of the variation in moments of $q_{\rm t} - q_{\rm sat}$ are due to those in $q_{\rm t}$. Interestingly, Fig. 2(a) indicates a weak anticorrelation between $S_{q{\rm t}}$ and $S_{q{\rm sat}}$ ($r = -0.42$, significant to 99% confidence with a t-test). The tethered-balloon data shows a similar result (significant to 97.5% confidence level). It is possible that this anticorrelation is linked with the covariance of T and q. A spectral decomposition of aircraft data (not presented) showed that T and q were anticorrelated on scales greater than about 1–5 km, consistent with previous findings (e.g. Williams *et al.* 1996). It is possible, therefore, that larger-scale processes are creating the observed skewness anticorrelation for the aircraft data. Conditional sampling of tethered-balloon data, however, shows cases where the anticorrelation between T and q extends down to the scale of clouds ($\sim$500 m, Price 1999). For example, moist cloudy air, having overshot its level of neutral buoyancy, was often seen to be surrounded by warmer drier air. The effect has also been observed in dry boundary layers. This provides an explanation for the observed anticorrelation of $q_{\rm t}$ and $q_{\rm sat}$ skewness and can be expected in the mid and upper regions of the boundary layer when thermals overshoot their height of neutral buoyancy, and also when entrainment introduces dry buoyant air there.

The data from the tethered balloon showed very similar results to those in Figs. 1–3. Figure 4 shows scatter plots of moments of $q_{\rm t}$ and $q_{\rm t} - q_{\rm sat}$ from balloon data for comparison with Figs. 1(c), 2(c) and 3(c).

Least-squares linear regressions were performed for the data shown in the scatter plots in Figs. 1–4 and the results from calculations of the gradient and its error are presented in Table 3. It can be seen that the gradients for standard deviation agree well between datasets. As indicated earlier, this suggests the possibility of a universal relationship. Data from arid boundary layers would be useful to test this further, since one might expect humidity variance there to be diminished relative to temperature, and produce a different gradient. This follows from the argument that for a convective boundary layer the ratio of $\sigma_{q{\rm t}-q{\rm sat}}/\sigma_{q{\rm t}}$ is expected to partly follow the ratio of sensible- to latent-heat flux, $\overline{w'T'}/\overline{w'q'}$, where w is vertical velocity (noting that it is also a function of the non-convective mesoscale gradients in T and q). The skewness and kurtosis gradients show less agreement between datasets and this indicates that the morphology of the two regions are not the same, as discussed above. Also presented in Table 3 are the correlation coefficients, which are generally high as expected. Note that they are progressively lower for the higher-moment correlations (though a t-test showed that all were significant to the 99.9% confidence level).

(*b*) *Spectral decomposition*

Since the aircraft data extend into the mesoscale they are suitable for spectral decomposition. Figure 5 shows the ratio of spectral power $q_{\rm sat}/(q_{\rm t} + q_{\rm sat})$ as a function of wave number. Similar results can be seen for the ASTEX and SATE-2 data, with little dependence of the ratio on length-scale down to approximately 100 m. Data from FIRE (which do not extend to small scales due to slow instrument response) indicate a similar invariance of the ratio with scale, but show a significantly higher mean value. This may indicate some geographical difference between the datasets. Additional data are also plotted for MAST (Monterey Area Ship Tracks experiment, see Durkee *et al.* 2000)

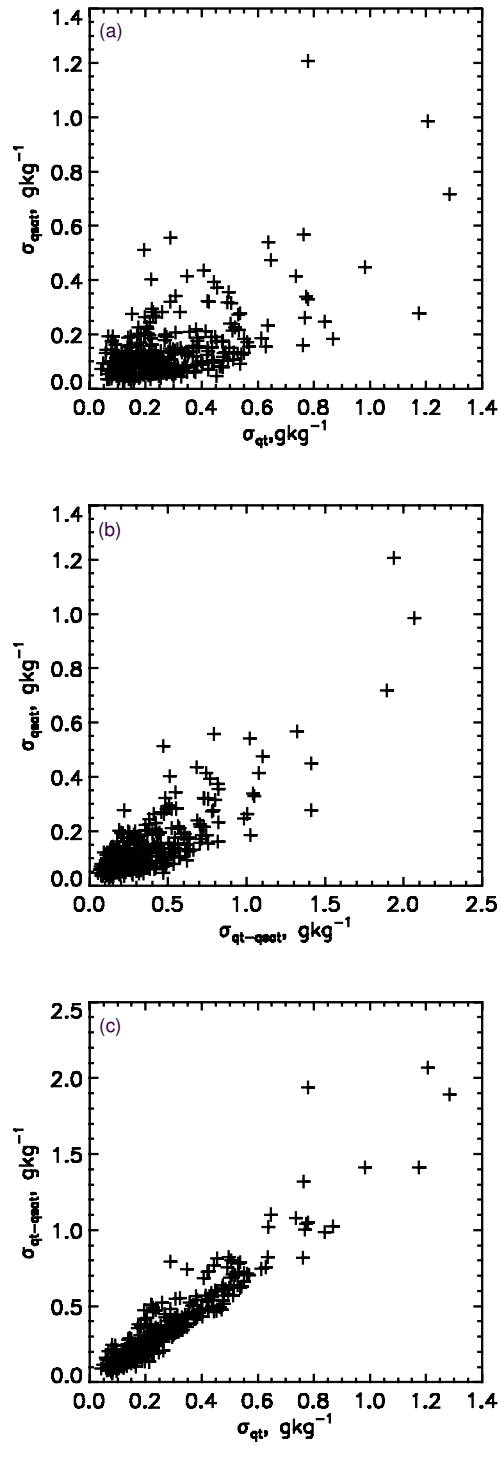

Figure 1. Scatterplots of aircraft data standard deviation for distributions of: (a) total specific humidity q_t, (b) saturation specific humidity q_{sat}, and (c) saturation deficit $q_t - q_{sat}$.

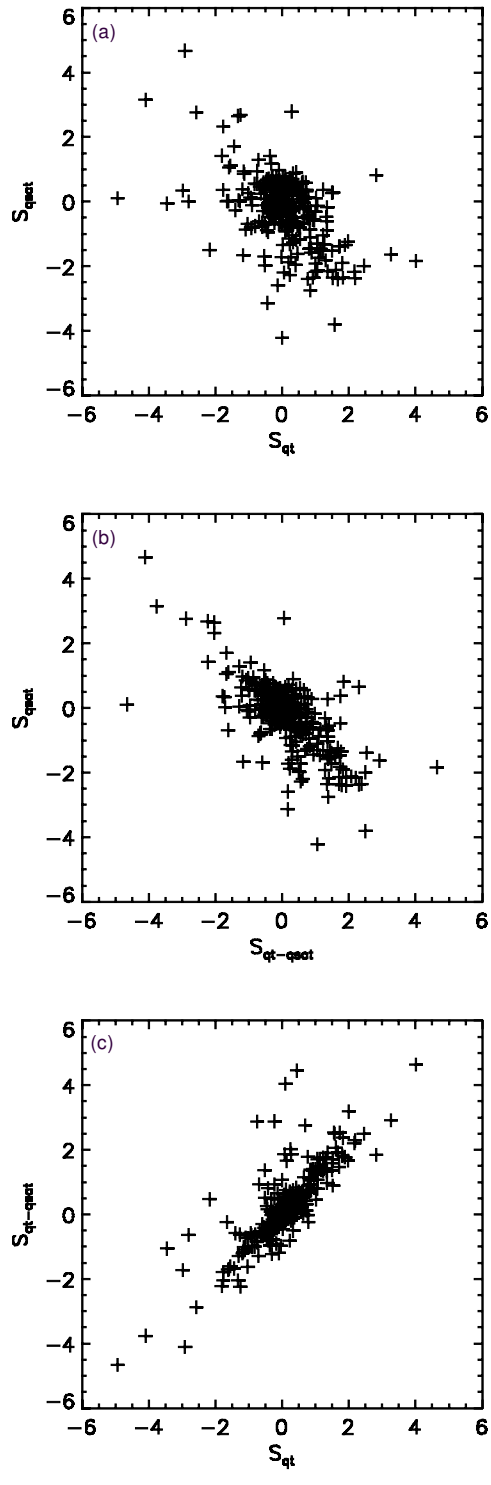

Figure 2. Scatterplots of aircraft data skewness for distributions of: (a) total specific humidity q_t, (b) saturation specific humidity q_{sat}, and (c) saturation deficit $q_t - q_{sat}$.

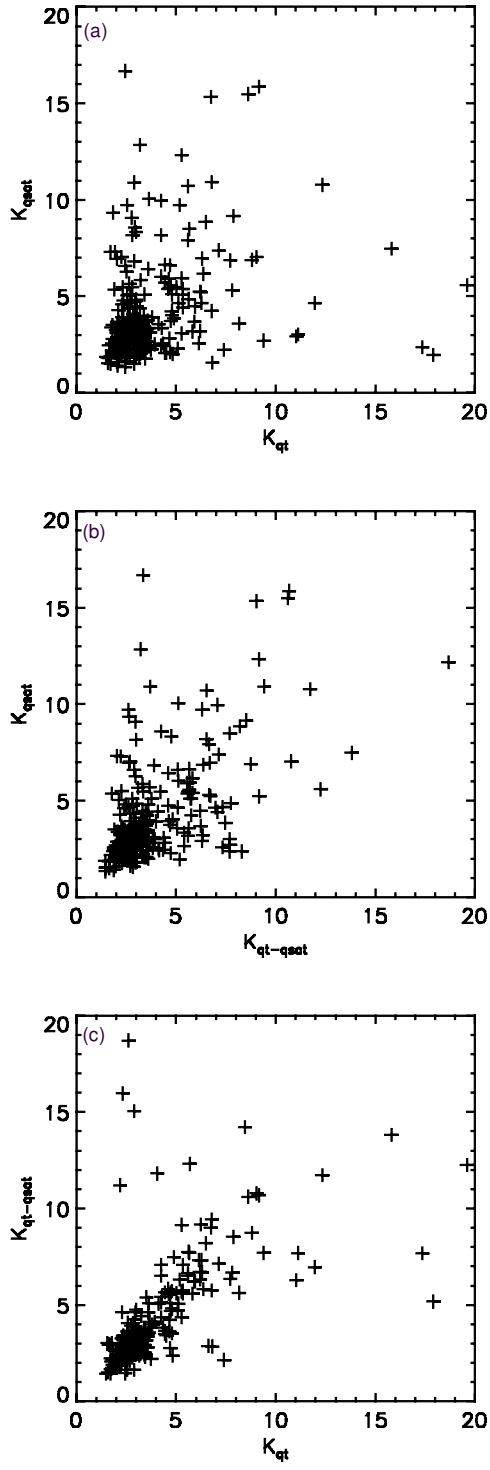

Figure 3. Scatterplots of aircraft data kurtosis for distributions of: (a) total specific humidity q_t, (b) saturation specific humidity q_{sat}, and (c) saturation deficit $q_t - q_{sat}$.

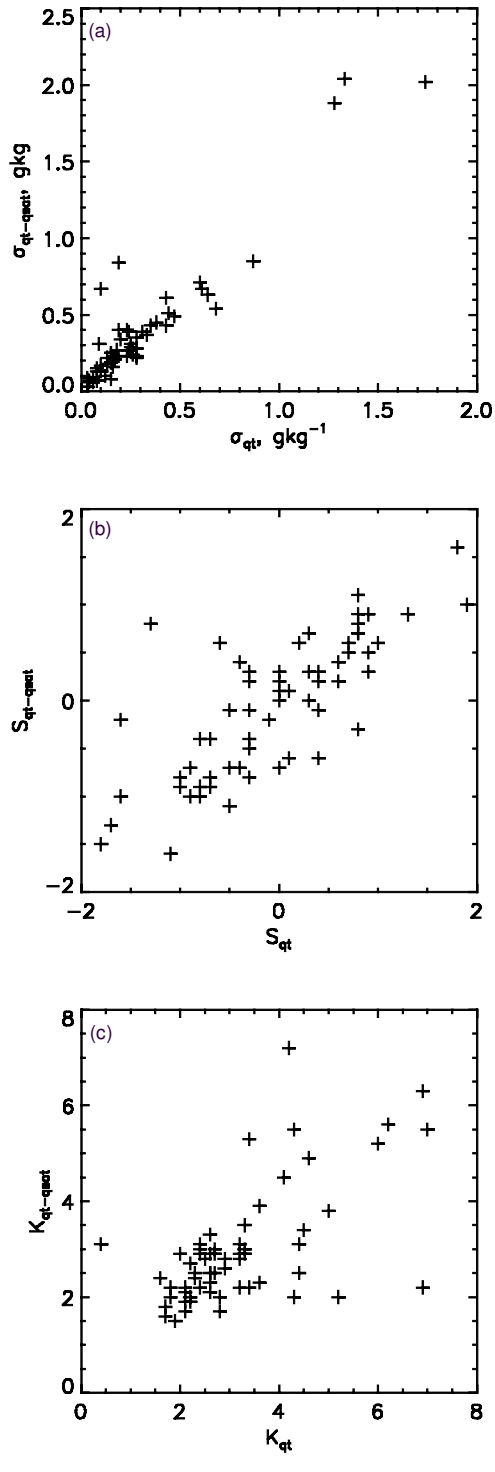

Figure 4. Scatterplots of tethered-balloon data: (a) standard deviation, (b) skewness and (c) kurtosis, for distributions of total specific humidity q_t, and saturation deficit $q_t - q_{sat}$.

TABLE 3. GRADIENTS OF MOMENTS WITH ERRORS AND CORRELATION COEFFICIENTS CALCULATED FROM LEAST-SQUARES REGRESSION OF $q_t - q_{sat}$ DISTRIBUTION AGAINST q_t DISTRIBUTION

Gradient	Aircraft	Correlation coefficient	Tethered balloon	Correlation coefficient
$\sigma_{qt-qsat}/\sigma_{qt}$	1.39 ± 0.26	0.93	1.21 ± 0.20	0.94
$S_{qt-qsat}/S_{qt}$	0.96 ± 0.32	0.83	1.39 ± 0.28	0.77
$K_{qt-qsat}/K_{qt}$	1.01 ± 0.32	0.82	0.55 ± 0.35	0.62

q_t is the total specific humidity, and $q_t - q_{sat}$ is the saturation deficit; S is skewness and K kurtosis.

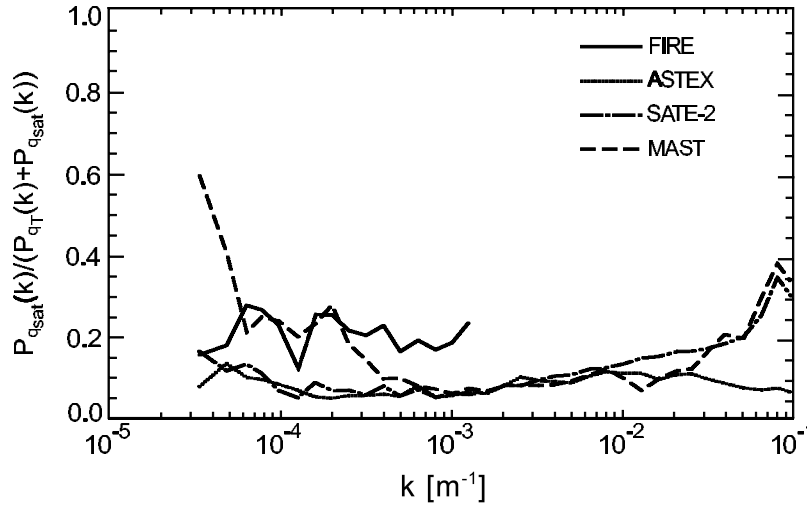

Figure 5. Spectral power, P, of the ratio $q_{sat}/(q_t + q_{sat})$ as a function of wave number, k, for aircraft data; where q_{sat} is the saturation specific humidity and q_t is total specific humidity.

which was designed explicitly to investigate the effects of effluent from ships on cloud morphology. The MAST trace in Fig. 5 shows significantly different properties to the other three, with a strong dependence on scale. The reason for this is not yet clear but must be linked to the relation between the mesoscale cloud structure and small-scale turbulence.

(*c*) *Associated errors in cloud fraction*

In this section the relative error in cloud fraction calculated from distributions in q_t compared to $q_t - q_{sat}$ are considered using the tethered-balloon data, which represent a reasonable sample of boundary-layer types. The definitions of cloud fraction for the two distributions of q_t and $q_t - q_{sat}$, are (respectively):

$$C_{qt} = \frac{\int_{q_{sat}}^{\infty} G(q_t)\, dq_t}{\int_{0}^{\infty} G(q_t)\, dq_t} \tag{1a}$$

and

$$C_{qt-qsat} = \frac{\int_{0}^{\infty} G(q_t - q_{sat})\, d(q_t - q_{sat})}{\int_{-\infty}^{\infty} G(q_t - q_{sat})\, d(q_t - q_{sat})}, \tag{1b}$$

where $G(\,)$ is the respective distribution function. In order to compare the two integrals directly for a given state of saturation one of the above integrals must be transformed.

This is done by adding $\overline{q_t} - \overline{q_t - q_{sat}}$ to $G(q_t - q_{sat})$ which aligns the mean values of the two distributions, and since $\overline{q_t - q_{sat}} = \overline{q_t} - \overline{q_{sat}}$ it is clear that both distributions will have their saturation point at q_{sat}. Equation (1a) can then be used for both distributions using the respective distribution function. This was done by binning each PDF into 100 values and allowing q_{sat} to take on each of those, allowing C_{qt} and $C_{qt-qsat}$ to be compared for cloud fractions between 0 and 1. For this study the relative error incurred by using the q_t distribution is defined as $C_{qt-qsat} - C_{qt}$.

Figures 6(a) and 7(a) show examples of contrasting comparisons of q_t and q_{sat} distributions. Figure 6(a) shows a PDF taken in a layer of quiescent wintertime Sc. Both distributions are narrow with only minor differences. In contrast Fig. 7(a) shows data from the upper part of a developing convective boundary layer, and illustrates a case where the two distributions were significantly different; the distribution including q_{sat} is much broader, with smaller kurtosis. These two examples show extremes of comparison; the majority of PDFs showed differences ranging between the two. Figures 6(b) and 7(b) show the calculation of relative cloud error as a function of cloud fraction for Sc and a developing convective boundary layer, respectively. It can be seen that the errors for the Sc data are significantly smaller than those for the convective boundary layer. Note that the actual cloud error is a strong function of the cloud fraction. This result is similar to that found when a PDF is fitted to the observed data and the predicted cloud fraction compared with that calculated from the observed PDF (Price 2001). Note that the mean (absolute) errors are significantly smaller than the peak errors, and vary between the two cases by more than an order of magnitude.

The mean relative cloud error for all 61 tethered-balloon data series is shown in Table 2 and is approximately half an okta. Note also that the standard deviation is relatively large which is consistent with the above discussion.

4. Conclusions

Comparisons of PDFs of specific humidity, q_t and saturation deficit humidity, $q_t - q_{sat}$, show a significant degree of proportionality between their moments. Their correlation coefficients decrease monotonically for the higher moments, as evident from the scatter plots presented in section 3. These indicate that most of the variation in the moments for the $q_t - q_{sat}$ distributions are governed by variations in the distributions of q_t. Spectral analysis of aircraft data suggest that these conclusions are largely independent of length-scale. The linear regressions of respective moments in q_t and $q_t - q_{sat}$ show that the estimated gradients for skewness and kurtosis differ significantly between aircraft and tethered-balloon datasets. This may be a consequence of different morphology between the atmospheric structure of midlatitude conditions over land and subtropical marine conditions. However, the gradient for standard deviation shows good agreement between the two datasets which indicates that there may be a universal correlation between σ_{qt} and $\sigma_{qt-qsat}$.

The relative error in cloud fraction calculated from distributions in q_t compared to $q_t - q_{sat}$ has been calculated. The results indicate that ignoring the variation of q_{sat} when calculating cloud fraction will incur an error, on average, of just less than half an okta. However, as noted in section 3, the standard deviation of the mean error calculated is relatively large, and therefore the actual range of errors encountered will be wide. In addition, since the error is also a function of cloud fraction one must expect a significant amount of variability in accuracy. Therefore, accurately predicting the distribution of $q_t - q_{sat}$ can be expected to produce superior predictions for cloud variables than using q_t only. However, since σ_{qt} and $\sigma_{qt-qsat}$ appear to be well correlated, parametrizations

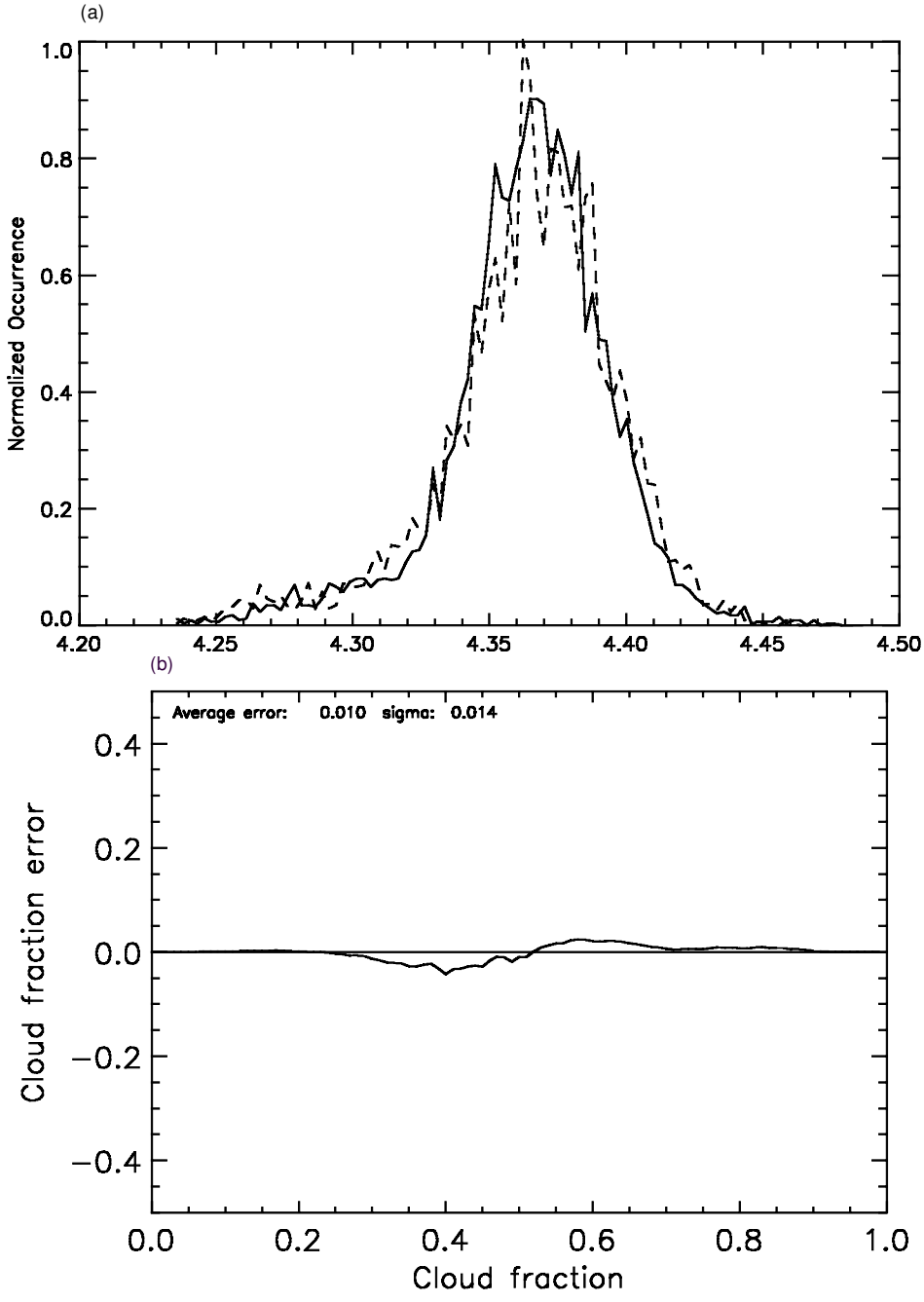

Figure 6. Examples of: (a) the comparison of total water (broken line) and saturation deficit (solid line) probability density functions for a wintertime case of stratocumulus, and (b) cloud errors as a function of cloud fraction invoked by neglecting variations in saturation specific humidity for a wintertime case of stratocumulus.

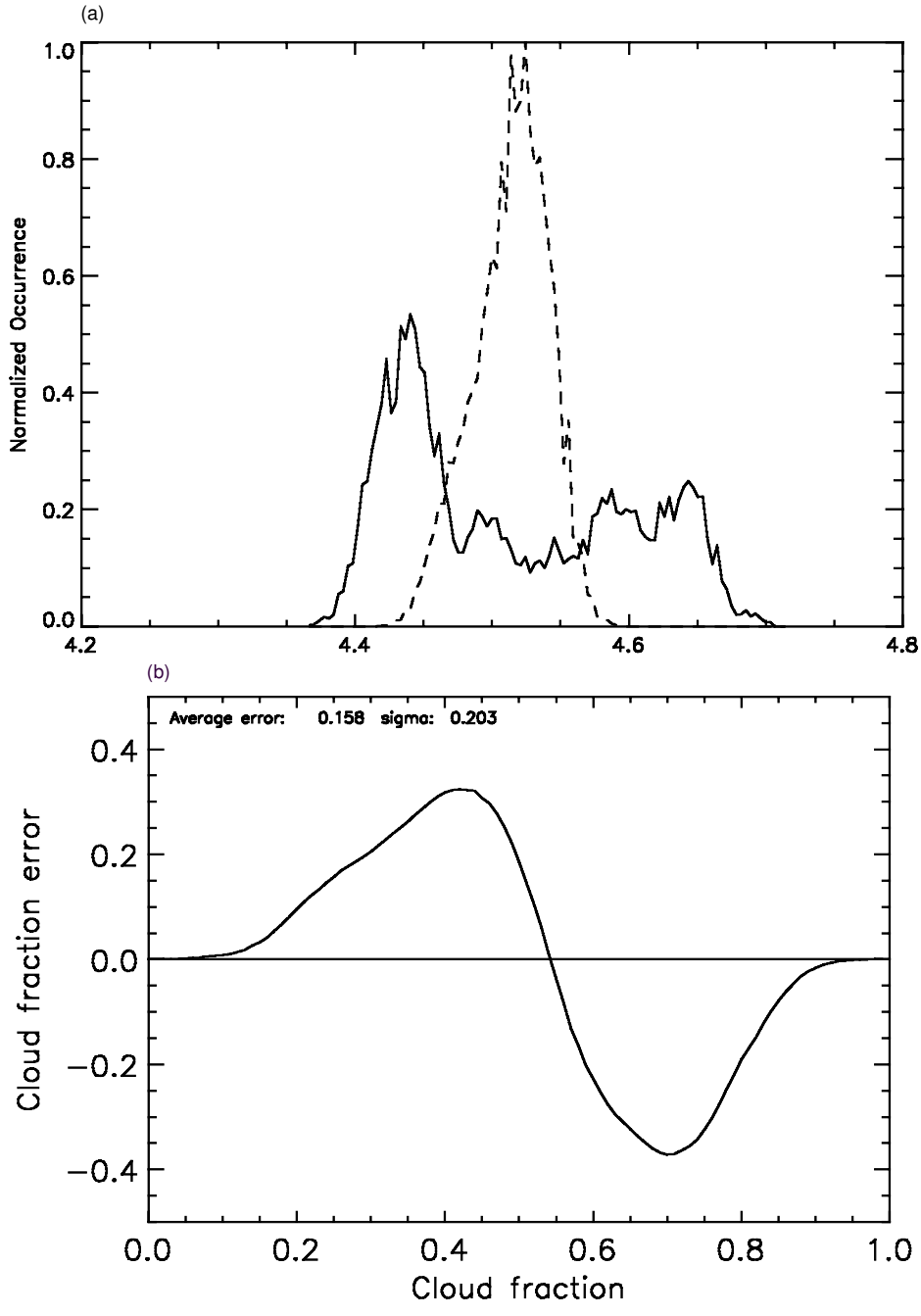

Figure 7. Examples of: (a) the comparison of total water (broken line) and saturation deficit (solid line) probability density functions for a summertime convective boundary layer, and (b) cloud errors as a function of cloud fraction invoked by neglecting variations in saturation specific humidity for a summertime convective boundary layer.

using σ_{qt} and $\sigma_{qt-qsat}$ can be considered interchangeable, with appropriate scaling. The observed differences between the gradients from the two datasets presented in Table 3 for higher moments, however, suggest a more complicated situation. Those moments might be interchangeable after consideration of any geographic and/or meteorological differences. Calculation of skewness however, is of secondary importance to standard deviation, as illustrated in Price (2001, see his Table 2), who showed that improper scaling of distribution width increased the mean error in cloud fraction of 61 data series by 44%. In contrast, not allowing for skewness produced an increase in error of 11%.

Finally, further examination of data over various geographical regions (particularly arid zones) would prove useful in determining whether the results found in this study are typical.

Acknowledgements

We would like to thank staff and flight crew at the Met. Research Flight, Farnborough and also staff at the Met. Research Unit, Bedfordshire, for their assistance in collecting the data. The comments of the two anonymous referees are also appreciated.

References

Bretherton, C. S. and Pincus, R. 1995 Cloudiness and marine boundary layer dynamics in the ASTEX Lagrangian experiments. Part 1: synoptic setting and vertical structure. *J. Atmos. Sci.,* **52,** 2707–2723

Cuijpers, J. W. M. and Bechtold, P. 1995 A simple parameterization of cloud water related variables for use in boundary layer models. *J. Atmos. Sci.*, **52,** 2486–2490

Cusack, S., Edwards, J. M. and Kershaw, R. 1999 Estimating the subgrid variance of saturation and its parametrization for use in a GCM cloud scheme. *Q. J. R. Meteorol. Soc.*, **125,** 3057–3076

Durkee, P. A., Noone, K. J. and Bluth, R. T. 2000 The Monterey Ship Track Experiment. *J. Atmos. Sci.,* **57,** 2523–2541

Ek, M. and Mahrt, L. 1991 A formulation for boundary-layer cloud cover. *Ann. Geophysicae*, **9,** 716–724

Francis, P. N. and Taylor, J. P. 1995 'SATE-2 Flight Summary'. Available from Met Office, Met. Research Flight, DERA, Farnborough, GU14 0LX, UK

Lapworth, A. J. and Mason, P. J. 1998 The new Cardingon balloon borne turbulence probe system. *J. Atmos. Oceanic Technol.*, **5,** 699–714

Larson, V. L., Wood, R., Field, P. R., Golaz, J.-C., Vonder Haar, T. H. and Cotton, W. R. 2001 Small-scale and mesoscale variability of scalars in cloudy boundary layers: One-dimensional probability density functions. *J. Atmos. Sci*, **58,** 1978–1994

Le-Treut, H. and Li, Z. X. 1991 Sensitivity of an atmospheric circulation model to prescribed SST changes: feedback effects associated with cloud optical properties. *Clim. Dyn.*, **5,** 175–187

Lohmann, U., McFarlane, N. Lekov, L., Abdella, K. and Albers, F. 1999 Comparing different cloud schemes of a single column model by using mesoscale forcing and nudging techniques. *J. Climate*, **12,** 438–461

Mellor, G. L. 1977 The Gaussian cloud model relations. *J. Atmos. Sci.*, **34,** 356–358

Pincus, R. and Klein, S. A. 2000 Unresolved spatial variability and microphysical process rates in large-scale models, *J. Geophys. Res.*, **105,** 27057–27065

Price, J. D. 1999 Observations of stratocumulus cloud break-up over land. *Q. J. R. Meteorol. Soc.*, **125,** 441–468

2001 A study on probability distributions of boundary layer humidity and associated errors in parametrized cloud fraction. *Q. J. R. Meteorol. Soc.*, **127,** 739–758.

Price, J. D., Jones, T. A. and Shields, J. 1998 A balloon borne instrument to measure total water content in low level clouds. *Meteorol. Apps.*, **5,** 351–357

Randall, D. A., Cookley, J. A., Fairall, C. W., Kropfl, R. A. and Lenschow, D. H. 1984 Outlook for research on subtropical marine stratiform clouds. *Bull. Am. Meteorol. Soc.*, **65,** 1290–1301

Ricard, J. L. and Royer, J. F. 1993 A statistical cloud scheme for use in an AGCM. *Ann. Geophysiae*, **11,** 1095–1115

Rogers, D. P., Johnson, D. W. and Friehe, C. A. 1995 The stable internal boundary layer over a coastal sea. Part I: airborne measurements of the mean and turbulent structure. *J. Atmos. Sci.*, **52,** 667–683.

Smith, R. N. B. 1990 A scheme for predicting layer clouds and their water content in a general circulation model. *Q. J. R. Meteorol. Soc.*, **116,** 435–460

Sommeria, G. and Deardorff, J. W. 1977 Subgrid-scale condensation in models of non-precipitating cloud. *J. Atmos. Sci.*, **34,** 344–355

Tompkins, A. 2002 A prognostic parametrization for the subgrid-scale variability of water vapour and clouds in large-scale models and its use to diagnose cloud cover. *J. Atmos. Sci.*, **59,** 1917–1942

Williams, A. G., Kraus, H. and Hacker, J. M. 1996 Transport processes in the tropical warm pool boundary layer. Part 1: spectral comparison of fluxes. *J. Atmos. Sci.*, **53,** 1187–1202

Wood, R. and Field, P. R. 2000 Relationships between total water, condensed water and cloud fraction in stratified clouds examined using aircraft data. *J. Atmos. Sci.*, **57,** 1888–1905